Batteries & Supercaps

Research Article
doi.org/10.1002/batt.202400654

Chemistry Europe
European Chemical Societies Publishing

www.batteries-supercaps.org

Bilayer Boost to UV Assisted Supercapacitors: Enhanced Performance with Transparent TiO_2/MoO_3 Heterojunction Electrode

Bhuvaneshwari Ezhilmaran,[b] Sreelakshmi Madhavanunni Rekha,[a] and Sarpangala Venkataprasad Bhat*[a]

Photo-assisted supercapacitor is a promising smart device component for achieving both energy conversion and storage. The photo-assisted functionality in a supercapacitor is realized through the choice of photo responsive electrode material under suitable illumination conditions. The well-known electrochemically active electrode materials are wide band gap semiconductors which absorb strongly in UV light. However, most of the prior studies on photo-assisted supercapacitors used visible light. Herein, we present a transparent TiO_2/MoO_3 bi-layer heterojunction made by simple solution process as an efficient electrode for photo-assisted supercapacitors under UV light illumination. The electrochemical performance of the electrode is significantly enhanced even with a less intense (0.05 mW/cm^2) UV light, compared to dark as well as the single layer electrode under same illumination condition. The highest areal capacitance of 63.25 mF/cm^2 at 0.1 mA/cm^2 is achieved, that surpasses most of the recent relevant reports. The synergetic effect of UV illumination and the built-in potential at the type II heterojunction interface encourages ion insertion and better collection of the photo-generated carriers. The unique bi-layer design also leads to better rate capability features. Thus, the work presents a new prospect for the development of transparent energy storage devices to be used in future smart technologies.

1. Introduction

Electrochemical energy storage technologies, which mainly include supercapacitors and batteries are of great importance due to their ability to harvest energy from traditional as well as renewable sources.[1] Supercapacitors have received enormous attention over batteries due to the benefits associated with cyclic life, charging-discharging rate, and power density.[1,2] In recent years, several strategies such as doping, tuning the morphology of active electrode, introducing additional active material have been applied to enhance the performance of supercapacitors and the improvements have also been observed. Owing to the environmental impact of CO_2 emission and ever increasing energy demand, a clean, eco-friendly and sustainable resource has become a better alternate to meet the energy crisis.[3,4] Solar energy, a significant renewable energy source that reaches the earth's surface is far higher than the global energy requirement.[3,5] The proper utilization of solar energy in energy storage devices such as supercapacitors is expected to take up the storage technologies to a next level. However, the research towards the renewable source based supercapacitors is relatively still in its early stage.[6–8] Photo-supercapacitors are the solar light based energy storage devices that consist of both solar cell and supercapacitors.[9–11] However, the main problems associated with these kind of integrated devices is the voltage mismatch and the complex device architecture, which could be partially overcome by utilizing the single active electrode material which has good photoelectric and capacitance characteristics.[12,13]

Supercapacitors that operate with renewable sources, for instance solar energy and solar thermal energy is gaining much interest due to its advantages and benefits over conventional devices as well as photosupercapacitors.[2,14–17] A semiconducting material sensitive to both light and electrochemical reaction is preferred as an active electrode material for photo-assisted energy storage devices. Zhu et al. investigated the supercapacitance performance of h-WO_3 upon illumination of solar light with different conditions and the enhancement of about 17% in the areal capacitance was achieved.[2] Following that, ReS_2,[14] Co_3O_4,[13] ZnO,[15] $Ni(OH)_2$,[16] Cu_2O[18] based electrodes have been studied as an active electrode and improvements in the performance were also observed. However, most of these investigations are limited to the white light illumination condition. We could understand from the literature that most of the active materials used in this kind of photo irradiation assisted supercapacitors are wide bandgap semiconductors that have larger absorption in the UV region compared to visible region. The UV sensitive supercapacitors can be coupled with low power outdoor devices that requires low power such as wireless gas monitors or sensors.[19] The strong absorbance in the UV region persists in these materials despite the effect of

[a] S. Madhavanunni Rekha, S. Venkataprasad Bhat
SRM Research Institute & Department of Physics and Nanotechnology, SRM Institute of Science and Technology, Kattankulathur, Chengalpattu, Tamil Nadu, India
E-mail: venkatab@srmist.edu.in

[b] B. Ezhilmaran
Current affiliation: Research Center for Advanced Materials Technology & School of Advanced Materials Science and Engineering, Sungkyunkwan University, Suwon, Gyeonggi-do 16419, Republic of Korea

Supporting information for this article is available on the WWW under https://doi.org/10.1002/batt.202400654

surface modification, heterostructure utilization etc on the absorption and band edge as reported. Very few studies on the photo assisted capacitors have been reported with suitable illumination conditions related to the optical characteristics of the active material, for instance, UV light.[15,20] Thus, we sought to explore the choice of illumination condition in accordance with the optical properties to clearly understand the effect of photons on the capacitance performance. Also, the UV absorbing active materials are visibly transparent and this transparency feature is considered as the heart of future smart electronic technology.

The research towards the development of transparent devices is never ending due to their wide application.[21–26] As energy storage devices are one of the key components in integrated electronics, transparent storage devices are essential to complete the fabrication of fully transparent electronic systems. However, the fabrication of transparent energy storage devices is still in the beginning stage. Supercapacitors which have the advantage of good cyclic stability, power capability and low-cost stand out as the best amongst various power sources. Moreover, there are only few studies reported on the transparent electrodes based supercapacitors which mostly employ organic materials.[6–8] Considering the advantages of inorganic materials and the importance of renewable energy, we believe that investigation of the capacitance performance of the inorganic material based transparent electrodes with light would pave a way forward in this direction.

The electrode design is one of the important factors to achieve good performance in both electrochemical and photoelectrochemical systems. For example, the use of more than one active material in a supercapacitor electrode yields better performance due to the junction formation at the interface.[15,16,27–29] In case of photo related devices the electrode should be carefully designed to efficiently collect the photogenerated carriers before recombination. Although a semiconductor generates additional carriers under suitable illumination, the carrier separation is significant for the photogenerated carriers to reach the electrodes where they are collected. In composite or core-shell model, the recombination rate would be relatively higher that should be minimal to achieve better performance.[30] Thus, the working electrode should be fabricated not only by considering the materials but also the interface design for photodriven supercapacitor applications. In this way, a bi-layer heterojunction structure would be a better option here, since the recombination rate would be relatively lower than that of the abovementioned models. Based on the photoelectric characteristics of 3 types of heterojunction, we could understand that the type II heterojunction at the interface will lead to better charge transfer and carrier separation.[27,30,31] Hence, a bi-layer electrode with type II junction at the interface is expected to exhibit better performance under proper illumination condition.

TiO_2 is a well-known semiconducting material which has been used in various energy harvesting and storage applications due to its high theoretical capacity, low cost, environment benign characteristics.[32–34] Also, the excellent photoelectric characteristics of TiO_2 make it one of the promising semiconductors in optoelectronic and photoelectrochemical systems. Hence, transparent TiO_2 based heterojunction electrode is expected to offer better performance. Orthorhombic MoO_3 is widely used in both energy conversion and storage applications due to its layered structure and favourable electronic properties. In addition, MoO_3 has a benefits of higher theoretical capacity, good electrochemical behaviour, high chemical stability.[35] Moreover, it makes type II heterojunction with TiO_2. Improved performance has been observed with TiO_2/MoO_3 heterostructures in various applications[36–41] including photocatalysis,[42] supercapacitors,[34] and photodetectors[43] as compared to TiO_2 or MoO_3 single material. However, the performance of TiO_2/MoO_3 heterojunction in photo-assisted supercapacitor is not reported, to the best of our knowledge. Herein, we report such a transparent electrode for photo-assisted supercapacitor application for the first time. The working ability of our TiO_2/MoO_3 heterojunction material under UV light has been investigated in our previous work.[36] The TiO_2/MoO_3 transparent bi-layer heterojunction electrode was fabricated with simple sol-gel and spin coating methods. The photoelectric characteristics and the effect of UV illumination on the capacitance performance were elaborated.

2. Results and Discussion

The XRD patterns of TiO_2, MoO_3 and TiO_2/MoO_3 confirmed the formation of anatase TiO_2 (JCPDS-21-1272) and α-MoO_3 (JCPDS-05-0508) (Figure 1a). The XPS survey spectrum of TiO_2/MoO_3 film that with major Mo and O at the surface (Figure 1b). The deconvoluted Mo 3 d spectrum of TiO_2/MoO_3 has revealed the predominant oxidation state of Mo^{6+} along with relatively weaker Mo^{5+} state (Figure 1c). The peaks at 235.8 eV and 232.6 eV are attributed to the Mo $3d_{3/2}$ and Mo $3d_{5/2}$ orbital electrons of Mo^{6+}, respectively.[37] The doublet peaks located at the lower binding energies of 235.1 and 231.5 eV belong to Mo^{5+} oxidation state,[44] indicating the presence of oxygen vacancies at the surface.[45] Figure 1d shows the deconvoluted O1s spectrum of the TiO_2/MoO_3 film. The high intense peak at 530.6 eV could be ascribed to the lattice oxygen and the peak located at 531.9 eV is related to the oxygen vacancies present at the surface of TiO_2/MoO_3 film. These oxygen vacancies are favorable to the enhancement in electrical conductivity as well as the improvement in the capacitance characteristics.[46]

The FE-SEM images showed the surface morphology of irregular spherical nanoparticles for TiO_2 and randomly arranged nanospike like structures for MoO_3 (Figure 2a, b & S1). The cross-section image of TiO_2/MoO_3 heterojunction clearly showed the formation of bilayer with TiO_2 (306 nm) and MoO_3 (262 nm) (Figure 2c). The HR-TEM image (Figure 2d) indicated the presence of different lattices nearby, corresponding to MoO_3 and TiO_2. The lattice spacing of 0.34 nm and 0.63 nm could be attributed to the (011) plane of TiO_2 and (200) plane of MoO_3 respectively. This result confirms the interface between them in our electrode.

Figure 3 shows the UV-vis absorbance and transmittance spectra of TiO_2, MoO_3& TiO_2/MoO_3 films. All the films had shown

Research Article
doi.org/10.1002/batt.202400654
Chemistry Europe
European Chemical Societies Publishing

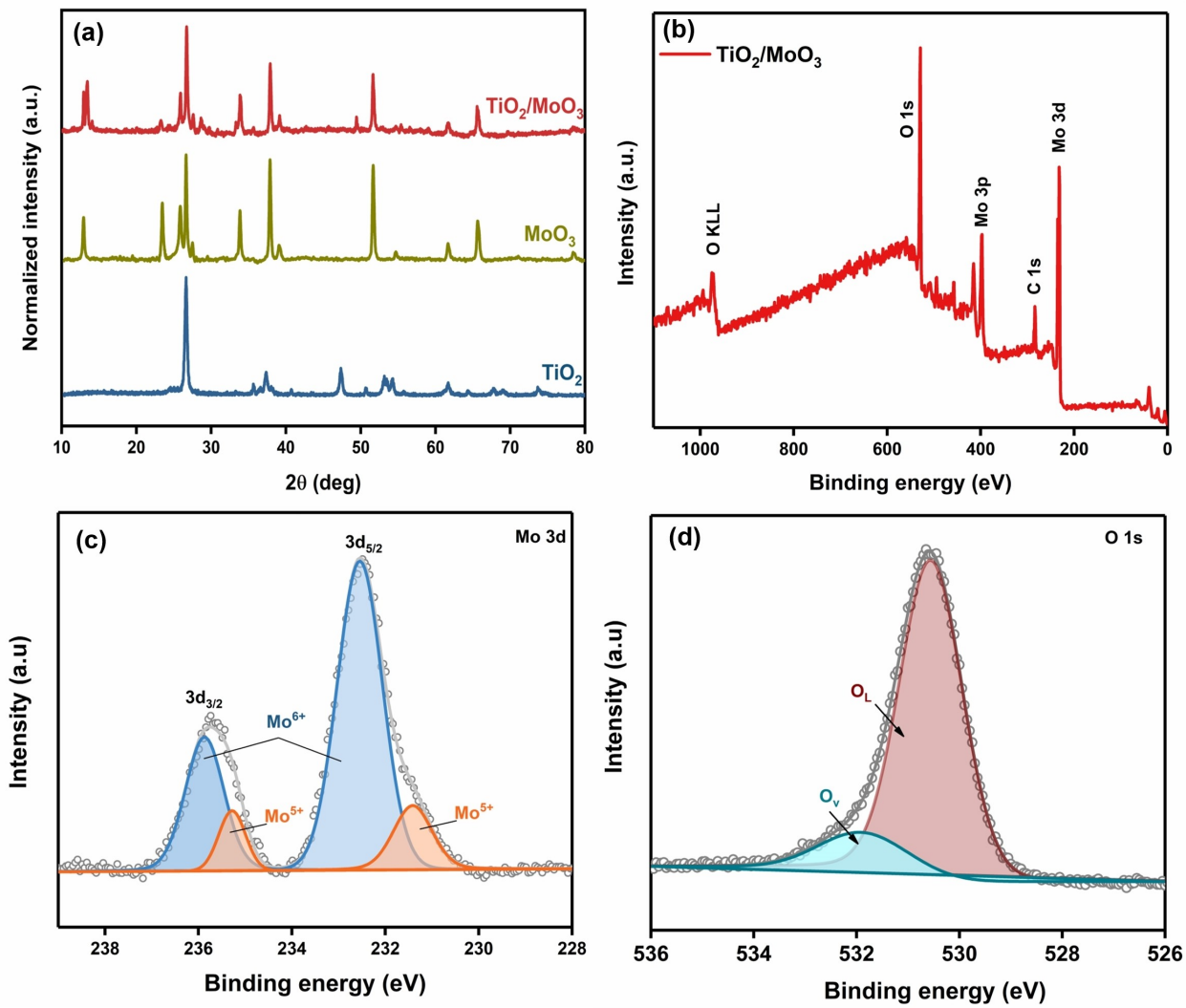

Figure 1. (a) XRD pattern of TiO_2, MoO_3 & TiO_2/MoO_3 films, (b) XPS survey spectrum, (c-d) High resolution XPS spectra (c) Mo3d and (d) O1s of TiO_2/MoO_3 film.

absorption in the UV region while transmitting visible light. The average transmittance in the visible region (420–800 nm) was estimated to be 87%, 85% and 78% for TiO_2, MoO_3& TiO_2/MoO_3 films respectively, exhibiting the transparent nature of the working electrodes.

The band alignment of TiO_2/MoO_3 was evaluated with XPS-VBM spectra and Tauc plot (Figure 4). The valence band maxima values were estimated to be 1.92 eV and 2.42 eV for TiO_2 and MoO_3 respectively. The conduction band values could be calculated by subtracting the band gap values with the valence band maxima values. Band gap Values (Eg) are calculated with Tauc plot considering the indirect transition for both materials. Eg is found to be approximately 3.3 eV for TiO_2 and 3.0 eV for MoO_3. The conduction band values could be estimated to be −1.38 eV and −0.6 eV for TiO_2 and MoO_3 respectively. Both valence and conduction band positions of TiO_2 are higher than that of MoO_3, confirming the formation of type II heterojunction at the interface. The built-in potential value could be expressed as the difference between the work function of the semiconductors. The work functions were estimated with scanning kelvin probe measurements and found to be 5.8 eV and 5.1 eV for TiO_2 and MoO_3 respectively. Hence, the estimated built-in potential at the interface is approximately 0.7 eV. The higher conduction band value of TiO_2 demonstrates the electron transfer could occur from TiO_2 to MoO_3, leaving net positive charges, whereas MoO_3 could have net negative charges at the interface. The absorption could take place on both TiO_2 and MoO_3 in the given UV radiation. The photogenerated carriers are migrated to the junction, where it gets separated. The electron could transfer from MoO_3 to TiO_2 and holes in the opposite direction due to the net charge effect.

The photoelectric characteristics of the electrodes were investigated by fabricating a photodetector device with thermally evaporated Au contacts (device structure: FTO/TiO_2/MoO_3/Au). The response was compared with bare TiO_2 and MoO_3 based devices (FTO/TiO_2/Au & FTO/MoO_3/Au). As all the films showed maximum absorption in the UV region, a 352 nm UV lamp was used as the light illumination source. Figure 5a show the semi-logarithmic plot of the I–V curves with the potential window of −0.5 to 0.5 V under dark and UV

Research Article
doi.org/10.1002/batt.202400654
Chemistry Europe
European Chemical Societies Publishing

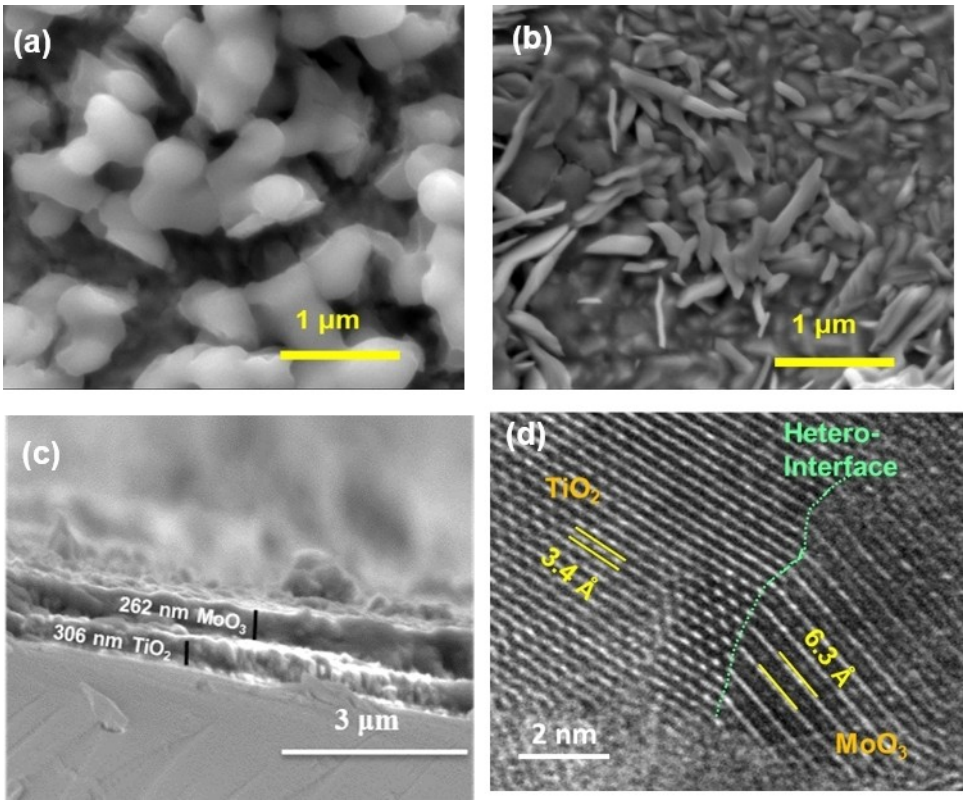

Figure 2. Surface SEM images of (a) TiO_2, (b) TiO_2/MoO_3, (c) cross section image of TiO_2/MoO_3 and (d) HR-TEM image of TiO_2/MoO_3.

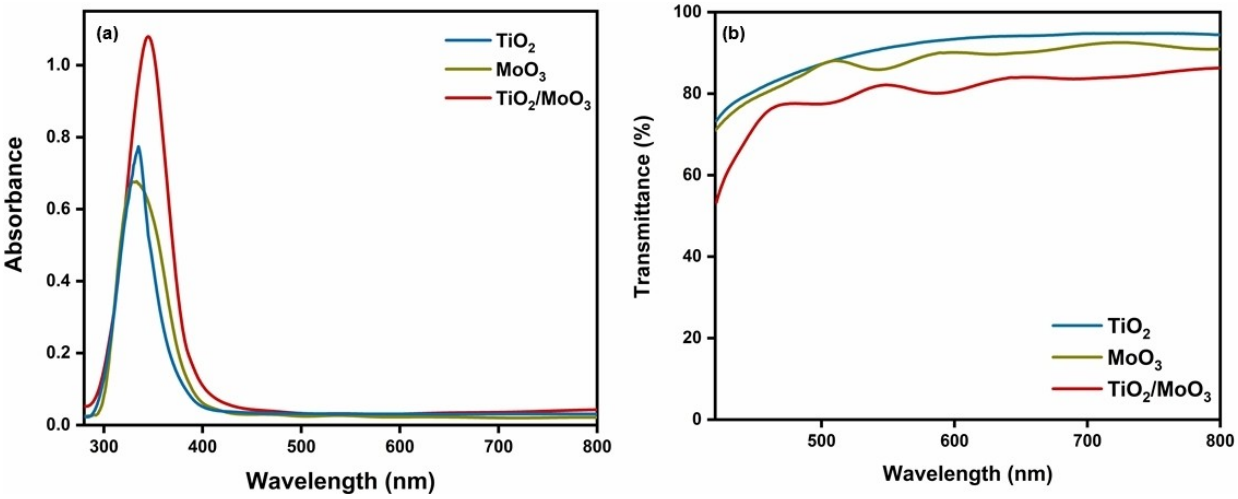

Figure 3. UV-vis (a) absorbance and (b) transmittance spectra of TiO_2, MoO_3 & TiO_2/MoO_3 films.

illumination for TiO_2 and TiO_2/MoO_3 respectively. It can be seen from the figures that the current obtained under UV light was higher than that obtained under dark condition. The additional current can be attributed to the photogenerated carriers. Though the additional carriers generated under UV illumination enhanced the current for both TiO_2 and TiO_2/MoO_3 based devices, it was much higher for the heterojunction based device as compared to the TiO_2 based device, confirming the relatively better generation and efficient separation of carriers in TiO_2/MoO_3. Since the photocurrent observed with MoO_3 based device was much lower (Figure S2), further measurements were limited to the devices based on TiO_2 and TiO_2/MoO_3. Further, to evaluate the role of the built-in potential on the separation of photogenerated carriers, the transient photocurrent measurements were done without an external bias. The I-t plots clearly explained the ability of light to provide additional carriers to enhance the current. The built in potential at the TiO_2/MoO_3 interface was responsible for the carrier separation and collection without any additional driving potential. The increment in the current was approximately 2 µA for the hetero-

Research Article
doi.org/10.1002/batt.202400654
Chemistry Europe
European Chemical Societies Publishing

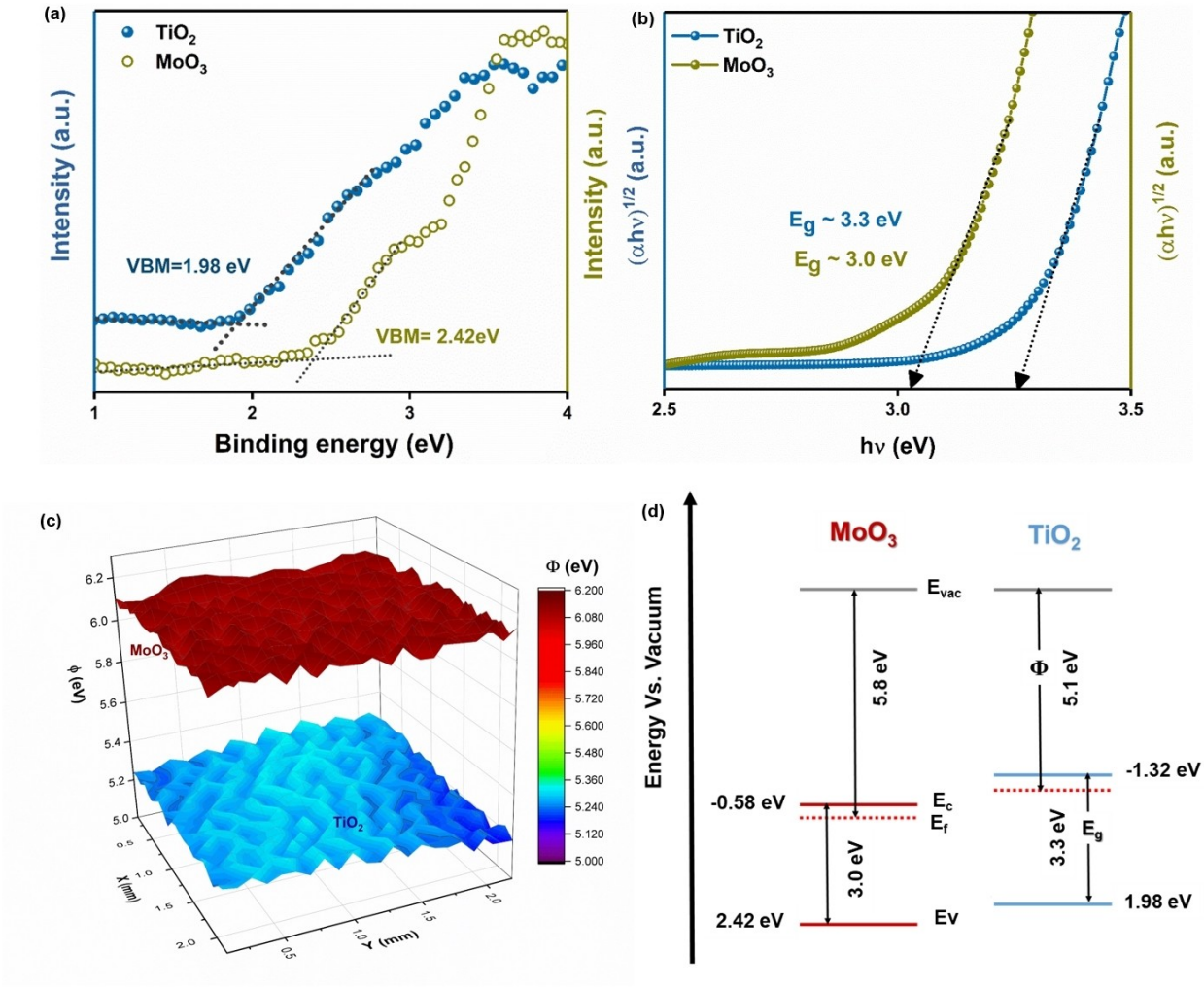

Figure 4. (a) XPS- Valence band maxima spectra, (b) band gap values, (c) Work function values of TiO_2 and MoO_3 films and (d) the band alignment diagram.

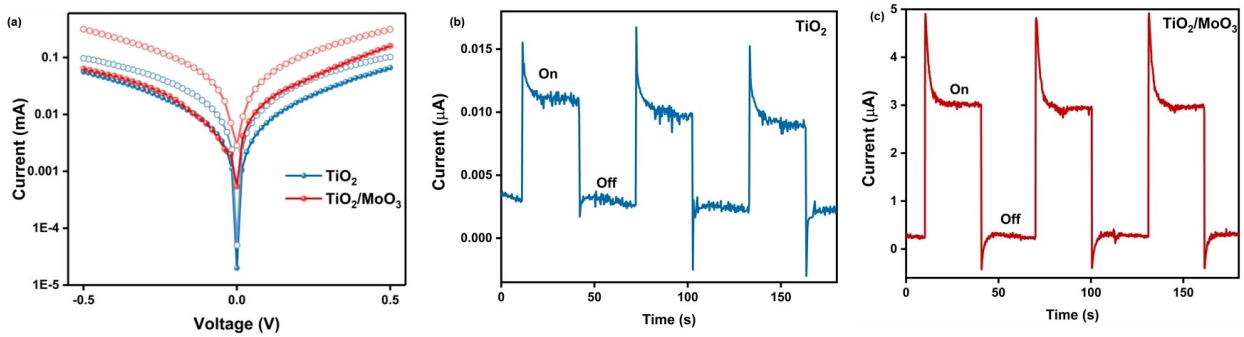

Figure 5. (a) Semi-logarithmic I–V plot under dark and UV light of TiO_2, TiO_2/MoO_3 based device, Transient photocurrent profile of (b) TiO_2 and (c) TiO_2/MoO_3 device without bias.

junction based device which was 3 orders higher than that of bare TiO_2 based device (Figure 5b &c). Hence, the addition of MoO_3 layer led to an enhanced optical absorption as observed with results of UV-vis absorbance measurements and subsequently this resulted in improved carrier generation. In addition, the type II nature of the heterojunction and the built-in potential at the TiO_2/MoO_3 interface led to better carrier separation and collection. Even in the case of bare TiO_2, the schottky junction at the FTO/TiO_2 interface led to the better separation and collection.[43] The results suggest that the TiO_2/MoO_3 heterojunction electrode can be used for photo-related applications. Further, the capacitance performance of the fabricated TiO_2&TiO_2/MoO_3 electrodes under dark and UV

Research Article
doi.org/10.1002/batt.202400654
Chemistry Europe
European Chemical Societies Publishing

illumination were investigated with cyclic voltammetry and galvanostatic charging–discharging profiles.

Upon light illumination, there is a possibility of hydrogen evolution or storage reaction to take place at more negative potential due to the acidic nature of the electrolyte used,[47] which could contribute to the current. Considering these facts, a narrow potential window of −0.5 to 0 V vs. Ag/AgCl was fixed for all the measurements. The cyclic voltammograms of TiO_2/MoO_3 heterojunction electrode at scan rates from 10 to 100 mV/s under dark and UV illumination conditions are shown in Figure 6a & b. The rectangular shape with evident redox peaks at all the scan rates exhibits the predominant Faradaic charge storage phenomenon. The CV curves at various scan rates showed similar shapes with broad cathodic/anodic peaks which could be related to the proton insertion/ extraction process. In addition, there was an increase in the current with increasing scan rate. The CV curves upon UV illuminations exhibited similar shapes to those under dark but with higher current, demonstrating the increased number of charges involved in the reaction. The area of the CV curve was also observed to be increased under UV illumination, indicating a large energy storage capability[2] (Figure 6c). The areal capacitance was calculated with the formula as mentioned below[14] and as expected, the capacitance was higher under light illumination condition.

$$C_a = \frac{\int I\, dV}{2A\ \Delta V\ \nu}$$

The integral part represents the area under the CV curve, A is the active area, ΔV is the voltage window, and ν is the scan rate. Figure 6d clearly depicts that the calculated value of capacitance under illumination was higher than that of observed under dark at all scan rates. For example, the capacitance calculated from the CV curve at the scan rate of 10 mV/s was 10.91 mF/cm^2 & 12.66 mF/cm^2 under dark and UV illumination respectively, exhibiting 16% enhancement, which correspond to the photoresponsive capacitance of 35 F/W (Equation S1). It's also noteworthy that the capacitance enhancement at all the scan rates was above 10%, proving the

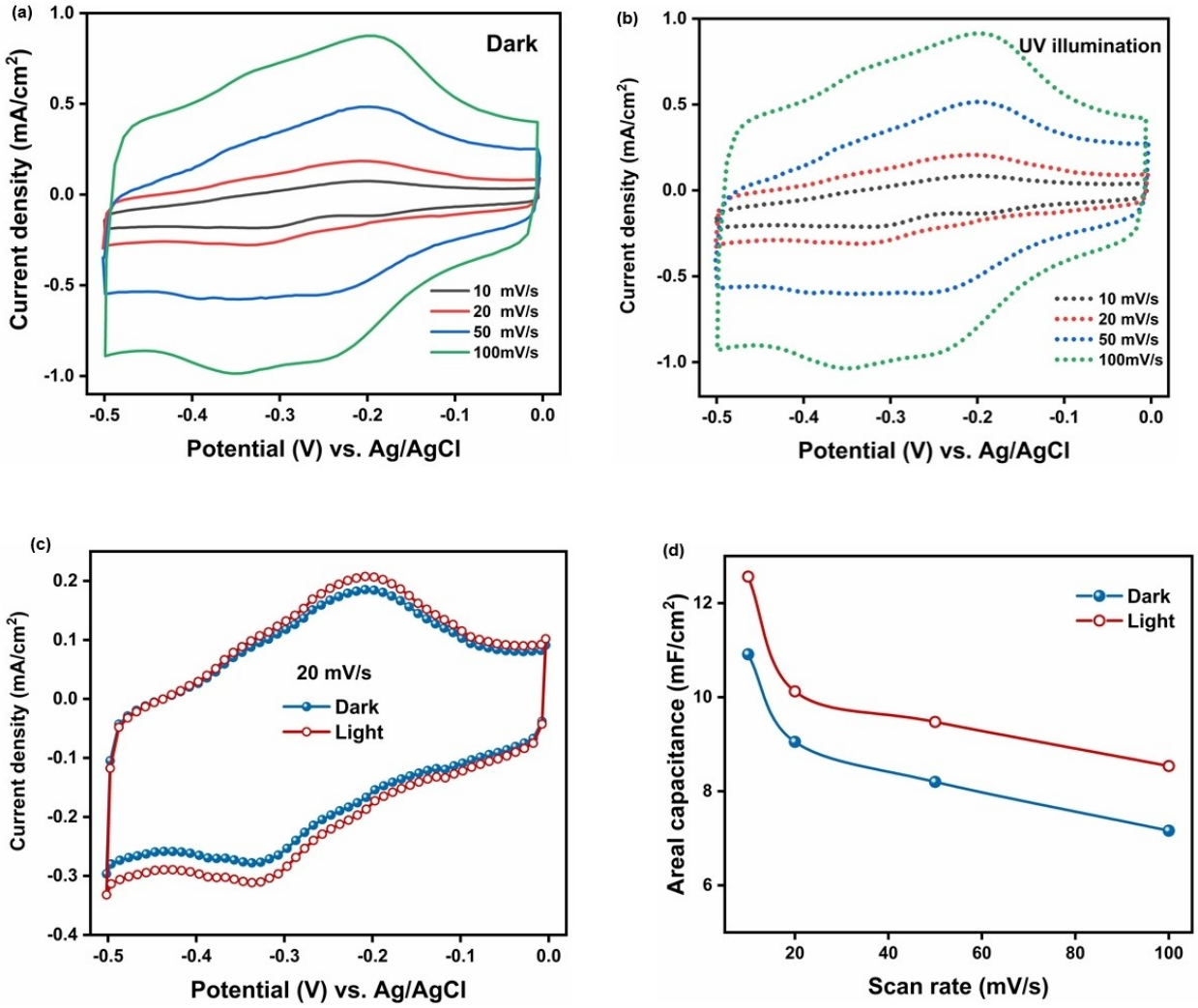

Figure 6. Cyclic voltammograms at different scan rates (a) under dark, (b) under UV illumination, (c) Cyclic voltammograms recorded at 20 mV/s under dark & UV illumination conditions and (d) The calculated areal capacitance at different scan rates of TiO_2/MoO_3 electrode.

ability of UV light to significantly enhance the charge storage characteristics of the transparent electrode.

Further, the storage mechanism under dark and light was investigated with CV measurements. As known, the electrochemical energy storage mechanism is classified into two ways: surface capacitive and diffusion controlled.[2] To understand the predominant process, b-value was primarily calculated by plotting log ν vs. log current following the fact that current at any fixed potential obeys power law,[2]

$$i = a\nu^b$$

where i, ν, a & b represents peak current, scan rate and adjustable numerals respectively. A b-value of 0.5 is known to denote the diffusion controlled process and a value of 1 denotes the surface capacitive mechanism.[48] Figure S3 (a & b) shows the calculated b-value for both anodic and cathodic peaks under dark as well as UV illumination conditions. It can be clearly seen from the figure that the deduced b-values were ranging from 0.68 to 0.73. The values near to 0.5 indicate the dominant diffusion controlled kinetics with the TiO_2/MoO_3 heterojunction. Also, the values were found to decrease (approaching 0.5) under illumination, indicating the improved diffusion controlled kinetics. To quantify the contribution of both surface and diffusion controlled charges to the total capacitance, the current at a fixed potential could be separated into two components based on the relation,[48]

$$i = k_1\nu + k_2\nu^{1/2}$$

where k_1 and k_2 are constants. The first term which is proportional to the scan rate ν denotes the capacitive contribution and the other term denotes the diffusion controlled current.[49] Figure S4 (c–d) show the capacitive and diffusion controlled currents under dark & UV illumination conditions. The results confirm that the diffusion controlled current was enhanced upon light illumination compared to that of dark. In contrast, the surface capacitive current was relatively decreased which is also in accordance with the b-values obtained. The contribution of diffusion-controlled current was increased almost 9% at all scan rates when UV light was irradiated. Hence, it can be deduced that the enhancement in capacitance was mainly due to the improved proton insertion and efficient separation of photogenerated charge carriers in the electrode upon UV illumination. This also indicates that the light illumination had a minimal impact on the adsorption of protons (surface capacitive process) at the electrode – electrolyte interface.[2] The photogenerated electrons would be the reason for the improved charge storage capabilities as observed in previous literature.[2,4,14,50–54]

Electrochemical impedance spectroscopy (EIS) analysis was performed to understand the change in the kinetics upon illumination. As we could see from the Figure S5 that The TiO_2/MoO_3 electrode exhibits relatively smaller charge transfer resistance (10.8 Ω) under light than that of dark (13.5 Ω), demonstrating the improved ionic and electrical conductivity.[13] In addition, a vertical line in the low-frequency region exhibits the better diffusion of charge carriers. Thus, the relatively improved charge transfer and diffusion characteristics might be attributed to the improved capacitance characteristics.[13,52]

Further, the galvanostatic charge/discharge (GCD) measurements were carried out at current densities ranging from 0.1 to 0.5 mA/cm^2 under dark & UV illumination conditions and the results are shown in Figure 7a & b. The charge/discharge time was improved under illumination compared to dark at all the applied current densities indicating the enhanced capacitance. Also, the difference in the shape of the curve was observed during the charging process, which could be related to the change in the charge storage mechanism upon UV illumination. It was noteworthy that, the symmetric nature of the GCD curve was greatly improved upon UV illumination indicating the improved ion insertion/extraction reversibility.[34] Figure 7c shows the charge/discharge profile under dark and illumination at the current density of 0.1 mA/cm^2. The total time consumed under dark was 233.9 s and the same under light was 487.4 s, exhibiting an increased capacitance. Though both charge and discharge time were increased, the increment in discharge time was almost double that of charging time, confirming the ability of light illumination to effectively enhance the charge storage (Figure S4). The areal capacitance with GCD was calculated with the formula,[14]

$$C_a = I\Delta t/\Delta Va$$

Where, C denotes the capacitance, I, Δt, ΔV, a are the applied current density, discharge time, potential window and active area of the electrode respectively. The calculated areal capacitance with TiO_2/MoO_3 electrode at 0.1 mA/cm^2 was 63.25 mF/cm^2 under UV illumination, which is 63.8% enhanced with respect to the capacitance achieved under dark (38.62 mF/cm^2). Unlike other reports, the enhancement percentage was almost same at all the current densities, which indicated that the photogenerated carriers effectively participate in the charge storage reaction irrespective of the applied current (Figure 7d). The rate capability was also found to improve upon light illumination.

To further understand the role of heterojunction on the performance, the capacitance characteristics of TiO_2 & TiO_2/MoO_3 electrode under dark and UV illumination was investigated through galvanostatic charging–discharging profiles. It can be clearly seen from the figure that the capacitance was much higher for the heterojunction electrode than bare electrode (Figure 6c). This could be attributed to the effective junction formation at the TiO_2/MoO_3 interface which expedited electron transfer, also provided the interfacial additional charge storage centres.[6] Figure S6 shows the calculated areal capacitance of TiO_2 & TiO_2/MoO_3 electrode under dark and illumination conditions at the current density of 0.1 mA/cm^2. The capacitance enhancement under light was relatively lesser for the TiO_2 (20.5%) electrode than the heterojunction electrode (63.8%). The improvement could be attributed to the improved carrier generation and efficient separation with type II heterojunction at TiO_2/MoO_3 interface.

Research Article
doi.org/10.1002/batt.202400654
Chemistry Europe
European Chemical Societies Publishing

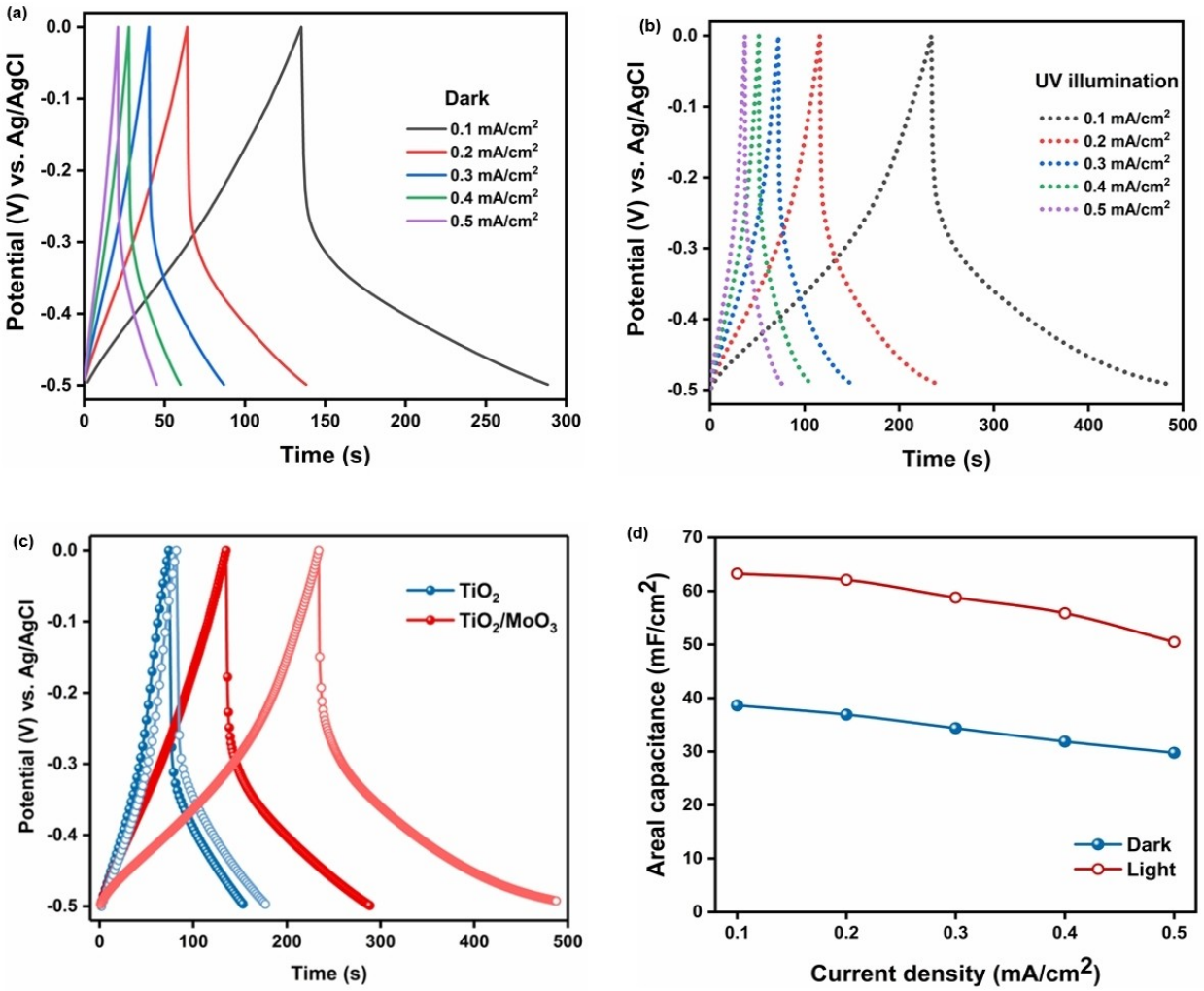

Figure 7. Galvanostatic charge-discharge (GCD) profiles: (a) at different current densities in the dark, (b) at different current densities under UV illumination, (c) comparison of TiO_2 and TiO_2/MoO_3 at 0.1 mA/cm^2 in the dark and under UV illumination, and (d) areal capacitance values at different current densities for the TiO_2/MoO_3 electrode under both dark and UV illumination conditions.

The capacitance kinetics under light could be elaborated as follows: When the TiO_2/MoO_3 electrode is irradiated with UV light, the electron hole pair generation takes place upon light absorption. Under an applied negative potential, the photo-generated carriers are separated. The photo generated electrons move towards the surface of the electrode while the holes move towards the counter electrode. The electrons then get neutralized by inserted protons.[2,15,16] Also, the UV light has the ability to improve the ionic conductivity that acts as a driving force for the active ions hence the amount of inserted proton would be improved. These additional photogenerated carriers and the improved active ions could be responsible for the observed increase in the current as well as the capacitance performance.[4,15,16] The improvement could be related to: (i) Acceleration of active ions by light energy, (ii) Involvement of photo-generated carriers in the energy storage process (iii) Improved carrier separation with bi-layer design assisted by the type II heterojunction at TiO_2/MoO_3 interface.

The cyclic stability of the TiO_2/MoO_3 electrode under light was tested with 500 CV cycles (Figure S7). The results showed a capacitance retention of 54%, demonstrating considerable cyclic stability. The long-term cycling under light promotes hydrogen evolution, evident as a tail at the lower potential after repeated cycles, which might be due to changes in the mass transfer characteristics at the electrode surface. The higher concentration of protons, coupled with light assisting hydrogen evolution even at lower potentials over time, contributed to these observations. The change in peak shape directly affects the area of the curve, thereby reducing the capacitance characteristics. The stability can be further improved by reducing the concentration of protons in the electrolyte. Having examined the electrode's enhanced performance under UV light, this cyclic stability analysis highlights the durability of the electrode over extended use, which is crucial for practical applications.

It can be seen from Table S1 that most of the studies reported are based on white light illumination and very few investigations have been made with UV light irradiation. However, transparent electrodes with suitable illumination conditions have not been reported to the best of our knowl-

edge. It is noteworthy that our electrode material exhibits superior areal capacitance value even with lesser illumination of 0.05 mW/cm^2 (Table S1). The enhancement percentage is higher than most of the electrode materials investigated under very high intensity. Also, our result stands out as the best among UV light assisted electrodes. The improved performance could be attributed to the bilayer heterojunction architecture of the electrode used. This approach could be also implemented with other photo responsive electrode materials for further improvements.

3. Conclusions

In summary, the photo-driven capacitance performance of a transparent TiO_2/MoO_3 heterojunction electrode fabricated with facile sol-gel and spin coating technique was investigated for the first time. The photoelectric characteristics of the TiO_2/MoO_3 electrode confirmed its ability to work effectively under UV illumination. The electrochemical performance of the device was greatly improved upon illumination. The highest areal capacitance of 63.25 mF/cm^2 at the current density of 0.1 mA/cm^{2}under UV light was observed, which was almost 1.6 times that of dark and 2.7 times of the bare TiO_2 electrode under same illumination conditions. Also, the device has exhibited good rate capability. The photogenerated carriers upon UV illumination which were then separated efficiently with type II heterojunction at the interface contributed towards the enhancement in the performance of the supercapacitor. Thus, its shown that a bi-layer heterojunction electrode designed suitably to the illumination conditions plays a significant role in improving performance of the photo-assisted capacitor and this opens the door to develop highly efficient solar driven supercapacitors as next generation transparent energy storage devices.

Experimental

Synthesis and Electrode Fabrication

TiO_2 and MoO_3 precursor solutions were made by following simple recipes reported in the literature[43] (See supporting information). Thin films were made on conducting FTO coated glass substrates by spin coating. First, the TiO_2 coating was done with the rotation speed of 3000 rpm for 30 sec. The film was dried at 100 °C for 10 minutes. After seven such successive coatings, the film was finally annealed at 500 °C for 1 hour under air atmosphere. MoO_3 solution was then coated upon the TiO_2 film with the speed of 2000 rpm for 30 sec followed by drying at 130 °C for 15 minutes. Similar to TiO_2, after seven coatings, the film was annealed at 380 °C for 1 hour.[2]

Characterization Details

X-ray diffraction was carried out using Cu Kα radiation (Powder X-ray Diffractometer, PANalytical, Xpert) with the diffraction angle varying from 10 to 80°. UV-visible absorbance and transmittance study was carried out using an Agilent Cary 5000 UV-visible spectrophotometer. FE-SEM analysis was carried out with a Quanta FEG 2000. A 352 nm UV lamp with the intensity of 0.05 mW/cm^2 was used as the illumination source for all the measurements. I–V and photocurrent measurements were carried out with a Keithley 2450 source meter unit. The electrochemical performances were analyzed in a 3-electrode configuration using Pt wire as counter electrode, Ag/AgCl electrode as reference electrode and 0.5 M H_2SO_4 aqueous solution as the electrolyte. The active area of the sample was 1 cm^2. All the electrochemical measurements were carried out using Squidstat plus, Admiral Instruments, USA.

Acknowledgements

The authors acknowledge the financial support of SRMIST towards this research work and all the in-campus characterization facilities such as the UV-visible spectrometer at the Department of Physics & Nanotechnology, FE-SEM facility at NRC and the XRD facility with the support from MNRE (Project No. 31/03/2014-15/PVSE-R&D), Govt. of India. We thank Prof. P. Malar and co-workers for the help with the use of a thermal evaporator. We thank Dr. S. Anandhakumar and Dr. V. Kumaran for their help with access to electrochemical workstation and electrodes. Thanks are due to Ms. Brahmari Shetty for the help with initial electrochemical measurements. This work was also supported by DST-SERB [File. No. ECR/2015/000513], MNRE [File. No. 31/03/2014-15/PVSE-R&D], Govt. of India and the Research Fund [R21-4181443579] from Royal Society of Chemistry, UK.

Conflict of Interests

The authors declare no conflict of interest.

Data Availability Statement

The data that support the findings of this study are available from the corresponding author upon reasonable request.

Keywords: Energy storage · capacitance · UV light · Heterojunction · Bilayer

[1] J. R. Miller, P. Simon, *Science* **2008**, *321*, 651–652, 10.1126/science.1158736.
[2] M. Zhu, Y. Huang, Y. Huang, Z. Pei, Q. Xue, H. Li, H. Geng, C. Zhi, *Adv. Funct. Mater.* **2016**, *26*, 4481–4490, 10.1002/adfm.201601260.
[3] P. V. Kamat, K. Tvrdy, D. R. Baker, J. G. Radich, *Chem. Rev.* **2010**, *110*, 6664–6688, 10.1021/cr100243p.
[4] H. Wang, J. Cao, Y. Zhou, Z. Wang, Y. Zhao, Y. Liu, H. Huang, M. Shao, Y. Liu, Z. Kang, *Nanoscale* **2020**, *12*, 17925–17930, 10.1039/d0nr05532h.
[5] N. Armaroli, V. Balzani, *Angew. Chem. Int. Ed.* **2007**, *46*, 52–66, 10.1002/anie.200602373.
[6] K. Poonam Sharma, A. Arora, S. K. Tripathi, *J. Energy Storage* **2019**, *21*, 801–825, 10.1016/j.est.2019.01.010.
[7] C. Zhao, W. Zheng, *Front. Energy Res.* **2015**, *3*, 1–11, 10.3389/fenrg.2015.00023.
[8] G. Wang, L. Zhang, J. Zhang, *Chem. Soc. Rev.* **2012**, *41*, 797–828, 10.1039/c1cs15060j.
[9] T. N. Murakami, N. Kawashima, T. Miyasaka, *Chem. Commun.* **2005**, 3346–3348, 10.1039/b503122b.

[10] J. Xu, Z. Ku, Y. Zhang, D. Chao, H. J. Fan, *Adv. Mater. Technol.* **2016**, *1*, 1–5, 10.1002/admt.201600074.
[11] C. Shi, H. Dong, R. Zhu, H. Li, Y. Sun, D. Xu, Q. Zhao, D. Yu, *Nano Energy* **2015**, *13*, 670–678, 10.1016/j.nanoen.2015.03.032.
[12] F. Wang, X. Wu, X. Yuan, Z. Liu, Y. Zhang, L. Fu, Y. Zhu, Q. Zhou, Y. Wu, W. Huang, *Chem. Soc. Rev.* **2017**, *46*, 6816–6854, 10.1039/c7cs00205j.
[13] Y. Zhao, X. Wang, H. Li, B. Qian, Y. Zhang, Y. Wu, *Chem. Eng. J.* **2022**, *431*, 133981, 10.1016/j.cej.2021.133981.
[14] N. Arya, P. Avasthi, V. Balakrishnan, *Nanoscale Adv.* **2021**, *3*, 2089–2102, 10.1039/d0na00901f.
[15] R. Sinha, N. Roy, T. K. Mandal, *Chem. Eng. J.* **2022**, *431*, 133915, 10.1016/j.cej.2021.133915.
[16] P. Chen, C. Cao, C. Ding, Z. Yin, S. Qi, J. Guo, M. Zhang, Z. Sun, *J. Power Sources.* **2022**, *521*, 230920, 10.1016/j.jpowsour.2021.230920.
[17] F. Yi, H. Ren, K. Dai, X. Wang, Y. Han, K. Wang, K. Li, B. Guan, J. Wang, M. Tang, et al., *Energy Environ. Sci.* **2018**, *11*, 2016–2024, 10.1039/c8ee01244j.
[18] C. An, Z. Wang, W. Xi, K. Wang, X. Liu, Y. Ding, *J. Mater. Chem. A* **2019**, *7*, 15691–15697, 10.1039/c9ta03707a.
[19] W. Y. Yi, K. M. Lo, T. Mak, K. S. Leung, Y. Leung, M. L. Meng, *A Survey of Wireless Sensor Network Based Air Pollution Monitoring Systems*, **2015**; Vol. 15, ISBN 8522603502.
[20] P. Pattananuwat, A. Khampuanbut, H. Haromae, *Electrochim. Acta* **2021**, *370*, 137741, 10.1016/j.electacta.2021.137741.
[21] C. G. Granqvist, *Appl. Phys. A Solids Surfaces* **1993**, *57*, 19–24, 10.1007/BF00331211.
[22] M. Grundmann, H. Frenzel, A. Lajn, M. Lorenz, F. Schein, H. Von Wenckstern, *Phys. Status Solidi Appl. Mater. Sci.* **2010**, *207*, 1437–1449, 10.1002/pssa.200983771.
[23] F. Fu, T. Feurer, T. Jäger, E. Avancini, B. Bissig, S. Yoon, S. Buecheler, A. N. Tiwari, *Nat. Commun.* **2015**, *6*, 1–9, 10.1038/ncomms9932.
[24] J. Xu, W. Yang, H. Chen, L. Zheng, M. Hu, Y. Li, X. Fang, *J. Mater. Chem. C* **2018**, *6*, 3334–3340, 10.1039/c8tc00550h.
[25] C. C. Chen, L. Dou, R. Zhu, C. H. Chung, T. B. Song, Y. B. Zheng, B. Hawks, G. Li, P. S. Weiss, Y. Yang, *ACS Nano* **2012**, *6*, 7185–7190, 10.1021/nn3029327.
[26] F. L. Schein, H. Von Wenckstern, M. Grundmann, *Appl. Phys. Lett.* **2013**, *102*, 092109, 10.1063/1.4794532.
[27] T. Fang, H. Hu, J. Liu, M. Jiang, S. Zhou, J. Fu, W. Wang, Y. Yang, *J. Phys. Chem. C* **2021**, *125*, 18734–18742, 10.1021/acs.jpcc.1c05639.
[28] T. Zhao, Z. Xing, Z. Xiu, Z. Li, S. Yang, Q. Zhu, W. Zhou, *Int. J. Hydrogen Energy.* **2019**, *44*, 1586–1596, 10.1016/j.ijhydene.2018.11.152.
[29] J. Tao, X. Yu, Q. Liu, G. Liu, H. Tang, *J. Colloid Interface Sci.* **2021**, *585*, 470–479, 10.1016/j.jcis.2020.10.028.
[30] T. Teranishi, M. Sakamoto, *J. Phys. Chem. Lett.* **2013**, *4*, 2867–2873, 10.1021/jz4013504.
[31] H. Sun, Y. J. Park, K. H. Li, C. G. Torres Castanedo, A. Alowayed, T. Detchprohm, R. D. Dupuis, X. Li, *Appl. Phys. Lett.* **2017**, *111*, 0–5, 10.1063/1.4999249.
[32] J. Resasco, H. Zhang, N. Kornienko, N. Becknell, H. Lee, J. Guo, A. L. Briseno, P. Yang, *ACS Cent. Sci.* **2016**, *2*, 80–88, 10.1021/acscentsci.5b00402.
[33] R. R. Prabhakar, T. Moehl, S. Siol, J. Suh, S. D. Tilley, *Chem. Mater.* **2020**, *32*, 7247–7253, 10.1021/acs.chemmater.0c01581.
[34] Q. Wang, C. Zhou, X. H. Yan, J. J. Wang, D. F. Wang, X. X. Yuan, X. N. Cheng, *Energy Technol.* **2018**, *6*, 2367–2373, 10.1002/ente.201800346.
[35] I. A. de Castro, R. S. Datta, J. Z. Ou, A. Castellanos-Gomez, S. Sriram, T. Daeneke, K. Kalantar-zadeh, *Adv. Mater.* **2017**, *29*, 1701619, 10.1002/adma.201701619.
[36] B. Ezhilmaran, S. V. Bhat, *Mater. Today Commun.* **2022**, *31*, 103497.
[37] B. Ezhilmaran, S. V. Bhat, *Chem. Eng. J.* **2022**, *446*, 136924, 10.1016/j.cej.2022.136924.
[38] D. Di Yao, M. R. Field, A. P. O'Mullane, K. Kalantar-Zadeh, J. Z. Ou, *Nanoscale.* **2013**, *5*, 10353–10359, 10.1039/c3nr03666a.
[39] Y. J. Chen, G. Xiao, T. S. Wang, F. Zhang, Y. Ma, P. Gao, C. L. Zhu, E. Zhang, Z. Xu, Q. H. Li, *Sens. Actuators B* **2011**, *155*, 270–277, 10.1016/j.snb.2010.12.034.
[40] B. Zhang, S. Sun, N. Shi, X. Liao, G. Yin, Z. Huang, X. Chen, X. Pu, *J. Alloys Compd.* **2019**, *820*, 153066, 10.1016/j.jallcom.2019.153066.
[41] C. Wang, L. Wu, H. Wang, W. Zuo, Y. Li, J. Liu, *Adv. Funct. Mater.* **2015**, *25*, 3524–3533, 10.1002/adfm.201500634.
[42] H. Liu, T. Lv, C. Zhu, Z. Zhu, *Sol. Energy Mater. Sol. Cells.* **2016**, *153*, 1–8, 10.1016/j.solmat.2016.04.013.
[43] B. Ezhilmaran, M. Dhanasekar, S. V. Bhat, *Nanoscale Adv.* **2021**, *3*, 1047–1056, 10.1039/d0na00780c.
[44] H. S. Kim, J. B. Cook, H. Lin, J. S. Ko, S. H. Tolbert, V. Ozolins, B. Dunn, *Nat. Mater.* **2017**, *16*, 454–462, 10.1038/NMAT4810.
[45] L. Huang, F. Zhang, Y. Li, H. Wang, Q. Wang, C. Wang, H. Xu, H. Li, *J. Mater. Sci.* **2019**, *54*, 5343–5358, 10.1007/s10853-018-03227-4.
[46] X. Zhang, X. Liu, Y. Zeng, Y. Tong, X. Lu, *Small Methods* **2020**, *4*, 1–18, 10.1002/smtd.201900823.
[47] D. E. Scaife, *Sol. Energy.* **1980**, *25*, 41–54, 10.1016/0038-092X(80)90405-3.
[48] C. Chen, Y. Wen, X. Hu, X. Ji, M. Yan, L. Mai, P. Hu, B. Shan, Y. Huang, *Nat. Commun.* **2015**, *6*, 6929, 10.1038/ncomms7929.
[49] V. Augustyn, J. Come, M. A. Lowe, J. W. Kim, P. L. Taberna, S. H. Tolbert, H. D. Abruña, P. Simon, B. Dunn, *Nat. Mater.* **2013**, *12*, 518–522, 10.1038/nmat3601.
[50] S. Safshekan, I. Herraiz-Cardona, D. Cardenas-Morcoso, R. Ojani, M. Haro, S. Gimenez, *ACS Energy Lett.* **2017**, *2*, 469–475, 10.1021/acsenergylett.6b00728.
[51] M. Mohsen Momeni, H. Mohammadzadeh Aydisheh, B. K. Lee, *Chem. Eng. J.* **2022**, *450*, 137941, 10.1016/j.cej.2022.137941.
[52] H. Wang, J. Cao, Y. Zhou, X. Wang, H. Huang, Y. Liu, M. Shao, Z. Kang, *Nano Res.* **2021**, *14*, 3886–3892, 10.1007/s12274-021-3309-z.
[53] Y. Zhao, Y. Zhang, X. Wang, H. Li, Y. Wu, *J. Power Sources.* **2022**, *542*, 231741, 10.1016/j.jpowsour.2022.231741.
[54] A. Khampunbut, S. Kheawhom, W. Limphirat, P. Pattananuwat, *Electrochim. Acta.* **2023**, *443*, 141979, 10.1016/j.electacta.2023.141979.

Manuscript received: October 5, 2024
Revised manuscript received: October 30, 2024
Accepted manuscript online: November 5, 2024
Version of record online: November 21, 2024